Hindawi
Advances in Meteorology
Volume 2024, Article ID 6633255, 15 pages
https://doi.org/10.1155/2024/6633255

Research Article

Sensitivity of WRF-Simulated 2 m Temperature and Precipitation to Physics Options over the Loess Plateau

Siliang Liu

School of Remote Sensing and Information Engineering, Wuhan University, Wuhan 430072, China

Correspondence should be addressed to Siliang Liu; lslrsgis@whu.edu.cn

Received 5 July 2023; Revised 22 March 2024; Accepted 28 March 2024; Published 2 May 2024

Academic Editor: Roberto Coscarelli

The current paper evaluates the weather research and forecasting (WRF) model sensitivity to five different combinations of cumulus, microphysics, radiation, and planetary boundary layer (PBL) schemes over Loess Plateau for the period 2015, in terms of 2 m temperature and precipitation. The WRF configuration consists of a 10 km resolution domain nested in a coarser domain driven by European Center for Medium-Range Weather Forecasts Reanalysis (ERA-Interim) data. The model simulated 2 m temperature and precipitation have been evaluated at daily and monthly scales with gridded observational dataset. The analysis shows that all experiments reproduce well the daily 2 m temperature, with overestimation particularly in the low-temperature range. Precipitation is less well simulated, with underestimation in all range, especially for intense rainfall. Comparing with ERA-Interim, WRF shows no clear benefit in simulating daily 2 m temperature while prominent improvement in simulating daily precipitation. WRF simulations capture the annual cycle of monthly 2 m temperature and precipitation with a warm bias and wet bias for most experiments in summer. Some reasonable configurations are identified. The "best" configuration depends on the criteria.

1. Introduction

Regional climate information is important for impact studies and climate change research. Comparing with global models, regional climate models (RCMs) are capable to produce climate simulation at higher spatial resolution with more realistic representation of surface heterogeneity and elevation. Therefore, RCMs are becoming the preferred tools for understanding climate at the regional scale [1–3].

Among RCMs developed by various institutes across the globe, the WRF model has been widely used by the science community for different regions [4–13]. It is also one of the RCMs being used for the coordinated regional climate downscaling experiment (CORDEX) [2] within the World Climate Research Program. A key feature of WRF is that it offers various physical parameterization schemes to be chosen [14]. However, there are limited guidance or experience on which configuration is suitable for a specific climate regime of simulated domain. In fact, there is no optimal configuration since model skill depends on the region, the parameter, the season, and the timescale, among others. Rather than identifying the best configuration for a given criterion, we may prefer to identify one or few configurations depicting satisfactory skills for multiple criteria.

The Loess Plateau, located in central northern China among the middle reach of Yellow River, occupies an area of over 640,000 km^2 land surface. It crosses arid, semiarid, and semihumid climate zones, with annual average temperature range of 4.3°C–14.3°C and average annual precipitation range of 200–750 mm from northwest to southeast [15]. Precipitation in the wet season (May through October) accounts for around 78% of the annual precipitation [16]. Regional climate information, particularly in terms of temperature and precipitation, is critical for the agricultural crop yield [17–20], hydrology, and water resources [21, 22]. Precipitation amount is critical important for rain-fed agriculture over this region, which accounts for 80% of the cultivated land [15]. In addition, extreme precipitation may lead to severe soil erosion over the Loess Plateau. Due to its

fragile ecological environment and geographic features, the Loess Plateau is sensitive to climate change [23, 24]. Future climate change may exert even greater impacts on soil erosion, restored vegetation, limited water resources, and agricultural production [25–27].

A previous modeling study [28] demonstrates that RegCM4.3 is able to reproduce both the spatial and temporal features of the regional climate over the Loess Plateau. However, it tends to produce cold biases during winter and day biases during summer. Other studies focusing on China [29–31] or the Loess Plateau [32] using WRF largely overestimate the precipitation amount over the plateau. To provide reliable regional information over this region, accurate simulation of historical climate is a critical step. However, climate simulation biases and their sensivitiy to physical options are still not well understood [30, 32–34]. Although there are numerous studies conducting multiphysical sensitivity assessment using WRF over different regions [4–14, 35–38], the literature focusing on the Loess Plateau is still limited, which deserves further exploration.

The objective of this study is to evaluate the skill of different physics scheme combinations in reproducing regional climate over the Loess Plateau. Toward this end, starting from a reference model setup, general model performance is evaluated for one year period, testing the effects of different physical options on the simulation performance of daily, monthly, and seasonal values of 2 m temperature and precipitation. The results will provide useful information for dismissing less efficient parameterization schemes and selecting a suitable model configuration in this region. The overarching aim is to provide a basis for long-term simulations, impact studies, and future projections.

2. Materials and Methods

2.1. Model Configurations. Version 4.0 WRF model is employed with two-way nested domains: (1) outer coarse domain with 7140 km by 4770 km extent at 30 km grid spacing, covering the entire China mainland and surrounding area and (2) inner domain with 1420 km by 1150 km extent at 10 km grid spacing, focusing on the study area Loess Plateau. The coverage and geography of these two domains is illustrated in Figure 1. 33 vertical levels are set from surface up to 50 hPa in a terrain following the sigma coordinate. The detailed options of physical schemes and land surface model are listed in Table 1.

Lateral boundary condition (BC) and initial condition for outer domain are provided by ERA-Interim reanalysis [39], with horizontal spatial resolution of $0.75^\circ \times 0.75^\circ$, temporal interval of 6h, and 37 original pressure levels from 1000 to 1 hPa. Prescribed sea surface temperature (SST) from this dataset is updated each 6h as lower boundary conditions for the portions of the domain over the ocean.

The WRF model provides various options for the parameterization of (i) microphysics (MIC), (ii) cumulus parameterization (CP), (iii) surface layer condition (SLC), (iv) land surface model (LSM), and (v) planetary boundary layer (PBL). To create a WRF physics ensemble, a reference run using configuration recorded in a previous paper [40] is taken as the baseline, named as EXP_CAM. Then, the option for each scheme was changed once a time. Finally, a series of sensitivity experiments were designed, namely, EXP_DUD, EXP_BMJ, EXP_AC2, and EXP_3C (Table 2). These experiments were all carried out forced by identical initial condition and lateral boundary for one year spanning from December 1, 2014, to December 31, 2015, with the last month of 2014 treated as the spin-up period. As a normal monsoon year, the year 2015 was selected based on the examination of the East Asian summer monsoon index. Moreover, in terms of 2 m temperature and precipitation, the year 2015 is identified as normal year when investigating the anomaly from decadal observations.

Table 1: Common configurations of the WRF model for all sensitivity experiments.

	D01	D02
Horizontal resolution	30 km	10 km
West-east	7140 km	4770 km
South-north	1420 km	1150 km
Vertical layers	33	33
Time step	90 s	30 s
Meteorological BC	ERA-interim	Parent domain (D01) ndown

2.2. CMFD Gridded Dataset. To evaluate the performance of WRF-simulated 2 m temperature and precipitation, the China meteorological forcing dataset (CMFD) downloaded from National Tibetan Plateau Data Center (https://data.tpdc.ac.cn) is utilized as reference. This newly released gridded meteorological dataset is developed with 0.1° spatial resolution at daily scale covering the period from 1979 to 2018 [41]. It is compiled based on gauge-observed data obtained from the China Meteorological Administration and other datasets such as satellite precipitation data and Global Land Data Assimilation System data [42]. High-resolution elevation data are introduced in the observed air temperature interpolation [42].

The gridded observation dataset described above is reprojected to Lambert projection and aggregated to 10 km in order to be consistent with WRF model outputs. Variables as daily 2 m temperature and daily precipitation are investigated, which are further aggregated into monthly and seasonal averaged values. The entire year is divided into the following four seasons: winter (December–Feburary, DJF), spring (March–May, MAM), summer (June–August, JJA), and fall (September–November, SON).

2.3. Evaluation Metrics. Evaluation is an important process in order to assess the performance of regional climate simulations. In this regard, three metrics are utilized, namely, bias, root mean squared error (RMSE), and Pearson's correlation coefficient (R) against gridded observations. These metrics are applied on daily time series of area-averaged value over the Loess Plateau, which are calculated as follows:

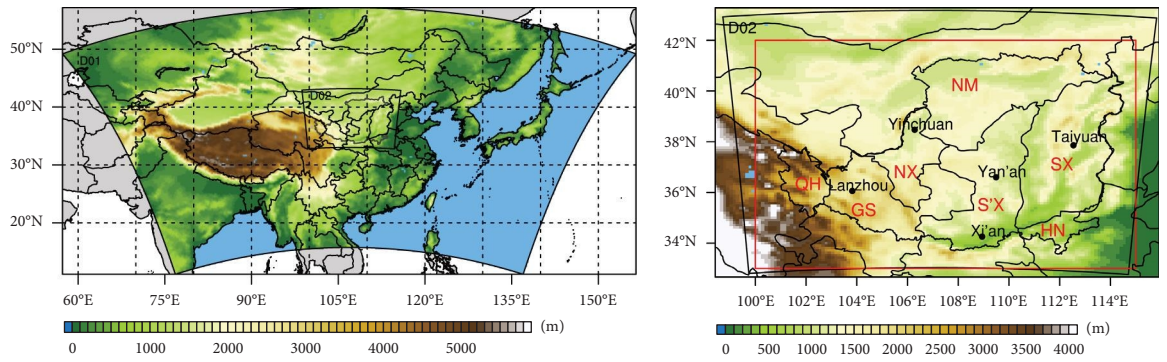

Figure 1: Domains used in the WRF simulations: (a) outer domain D01 and (b) inner domain D02. The rendered colormap denotes the elevation. The Loess Plateau is enclosed by the black border. The region includes seven provinces namely Neimeng (NM), Ningxia (NX), Shan'xi (S'X), Shanxi (SX), Henan (HN), Gansu (GS), and Qinghai (QH). The red rectangle covers the region to be analyzed in this study. The black dots represent several major cities in this area.

Table 2: Complementary configurations of the WRF model for sensitivity experiments.

Experiment	LSM	LW	SW	CP	PBL/SLC	SST	MIC
EXP_CAM	Noah	CAM	CAM	KF	YSU	ERAI	WSM6
EXP_DUD	Noah	RRTMG	Dudhia	KF	YSU	ERAI	WSM6
EXP_BMJ	Noah	RRTMG	RRTMG	BMJ	YSU	ERAI	WSM6
EXP_AC2	Noah	RRTMG	RRTMG	KF	AC2	ERAI	WSM6
EXP_3C	Noah	RRTMG	RRTMG	KF	YSU	ERAI	WSM3

$$\text{bias} = \frac{\sum_{i=1}^{n}(s_i - o_i)}{n}, \tag{1}$$

$$\text{RMSE} = \sqrt{\frac{\sum_{i=1}^{n}(s_i - o_i)^2}{n}}, \tag{2}$$

$$\text{R} = \frac{\sum_{i=1}^{n}(s_i - \bar{s})(o_i - \bar{o})}{\sqrt{\sum_{i=1}^{n}(s_i - \bar{s})^2}\sqrt{\sum_{i=1}^{n}(o_i - \bar{o})^2}}, \tag{3}$$

where s_i is the modeled value; o_i is the observation-derived value; and n is the number of grids.

Due to limited computation resources, the evaluation was conducted for the period of one single year 2015. The model quality assessment procedure focused on the capacity of the WRF runs to correctly represent the spatial and temporal structures of 2 m temperature and precipitation distributions. Therefore, the metrics were calculated for each grid box and accumulation period at daily scale for the current study against the correspondent regular gridded datasets.

2.4. Taylor Diagram. To evaluate the performance of different WRF configurations in simulating climatic conditions, the Taylor diagram [43] was generated for intercomparison in each season. It provides a concise statistical summary of spatial correlation (PCC), centered root-mean-square error (RMSE), and spatial standard deviation (STDV). Geometric relationship between these metrics allows that the performance of each configuration in comparison to reference can be displayed on the same diagram. A perfect simulation would be one with a centered RMSE equal to 0 and both the PCC and STDV close to 1. The azimuthal position of a symbol in the Taylor diagram gives information on the spatial correlation coefficient between the RCM results and the reference. The radial distances from the origin to each symbol are proportional to the pattern standard deviation normalized by the reference variance, thus reference located at value 1. The distances of each symbol (along concentric circles) from this reference point indicate the centered RMSE based on the RCM and reference data. The Taylor diagram reported in the present study was based on daily 2 m temperature and daily precipitation for area-averaged mean values, with CMFD-gridded observation as the reference.

3. Results

3.1. 2 m Temperature

3.1.1. Geographical Distribution of 2 m Temperature Bias. Figure 2 provides an overview on the spatial distribution of observed mean seasonal values and biases of ERA-Interim as well as WRF experiments and ensemble for average 2 m temperature. Observed 2 m temperature shows clear seasonal cycle, with highest values in JJA (20°C–28°C) and lowest in DJF (–10°C–6°C). The temperature decreases from south to north in general, with the highest in Guanzhong plain located at southern border and lowest in elevated west corner within QH province. In general, the WRF simulations reproduce well the spatial variability of 2 m temperature for

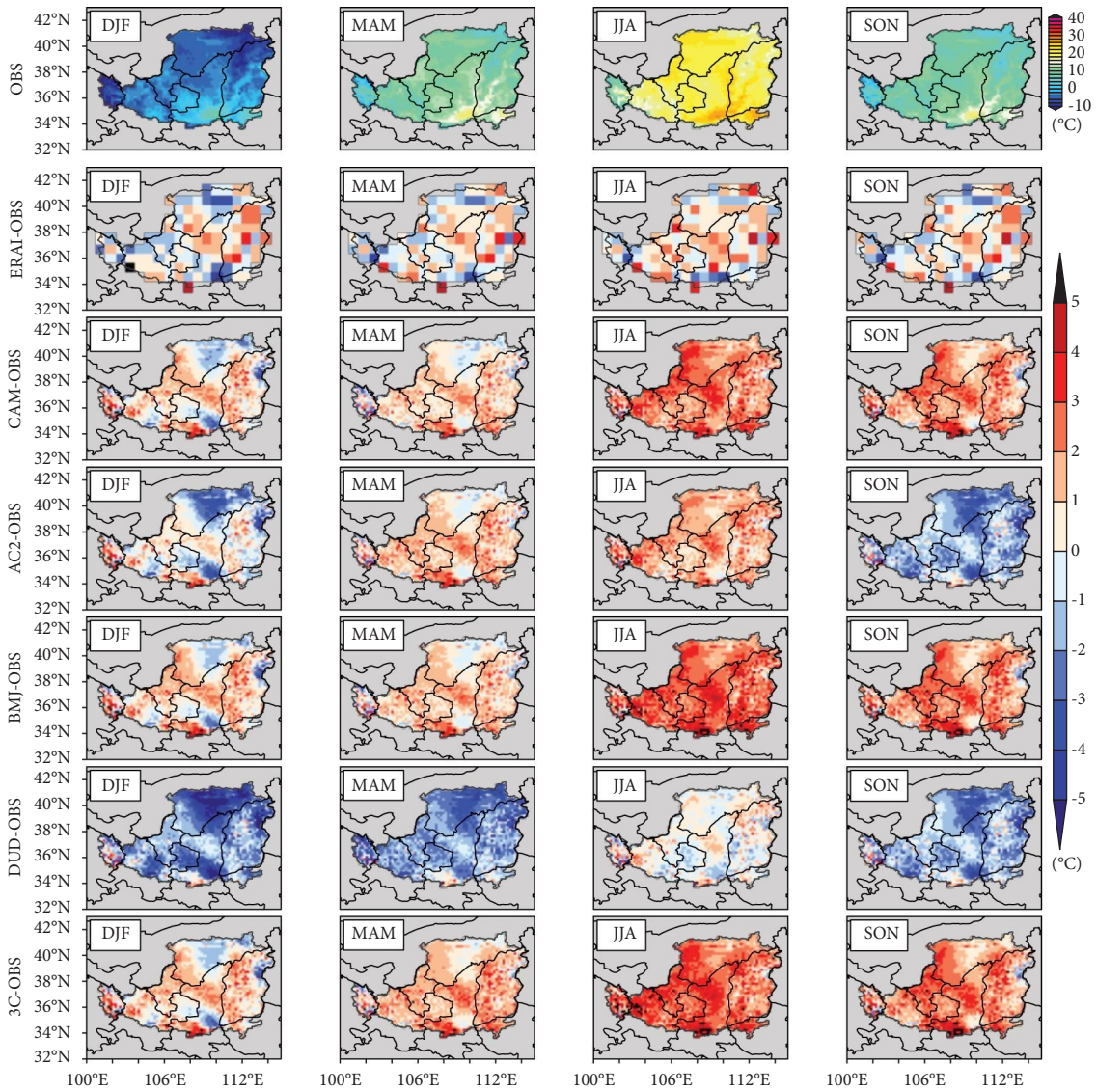

Figure 2: Seasonal mean observed 2 m temperature and bias of ERA-Interim reanalysis and WRF simulations. The first row shows 2 m temperature provided by the CMFD-gridded observation dataset as reference.

each season. In comparison with ERA-Interim, WRF simulations produce more spatial details. The WRF simulations present similar bias patterns except EXP_DUD. EXP_DUD shows prominent cold bias over almost the entire plateau in DJF, MAM, and SON (with the exception of small regions as the southern corner and western elevated area), while slight positive or negative bias over the entire plateau in JJA. The other four WRF simulations all produce strong warm bias in JJA with similar patterns but different magnitude (the areas with lower elevation seem correspond to higher warm bias) while both positive and negative bias in DJF, MAM, and SON depending on the regions.

The statistics of 2 m temperature at seasonal scale for each individual WRF experiments are summarized in Table 3. It can be identified that the correlation coefficients are commonly over 0.90 (except 0.88 for EXP_AC2 and EXP_DUD in DJF) for WRF simulations, which are higher in JJA and MAM as compared with SON and DJF. They are higher than the correlations for ERA-Interim in all four seasons (among 0.74–0.80), which indicates the added value of dynamical downscaling. Cold biases are prominent for EXP_DUD, particularly in DJF (−2.2°C), MAM (−1.9°C), and SON (−1.6°C). They are also large for EXP_AC2, in DJF (−0.8°C) and SON (−1.6°C). RMSEs are usually among the range between 0.20 and 0.50°C.

3.1.2. Annual Cycle of Monthly Mean 2 m Temperature. Figure 3 shows the annual cycle of area-average WRF-estimated 2 m temperature, together with the observation and ERA-Interim. The ensemble mean of the individual experiments are also calculated and presented. Overall, WRF simulations generate a good reproduction of observed monthly variation of 2 m temperature. The observation is generally within the range of model spread.

Table 3: Statistics of seasonal metrics for ERA-Interim reanalysis and WRF experiments in simulating daily 2 m temperature.

	DJF			MAM			JJA			SON		
	BIAS	RMSE	CORR	BIAS	RMSE	CORR	BIAS	RMSE	CORR	BIAS	RMSE	CORR
ERA-Interim	0.12	0.34	0.80	0.21	0.33	0.76	0.58	0.35	0.80	0.29	0.33	074
EXP_CAM	0.66	0.25	0.91	0.82	0.22	0.94	2.22	0.38	0.95	1.71	0.33	0.92
EXP_AC2	−0.80	0.31	0.88	1.12	0.24	0.94	1.54	0.29	0.96	−1.60	0.32	0.90
EXP_BMJ	0.83	0.26	0.91	1.00	0.23	0.94	2.69	0.45	0.95	1.92	0.36	0.92
EXP_DUD	−2.22	0.45	0.88	−1.93	0.35	0.94	0.12	0.17	0.95	−1.60	0.32	0.90
EXP_3C	0.81	0.26	0.91	1.41	0.28	0.94	2.69	0.45	0.95	2.00	0.37	0.92

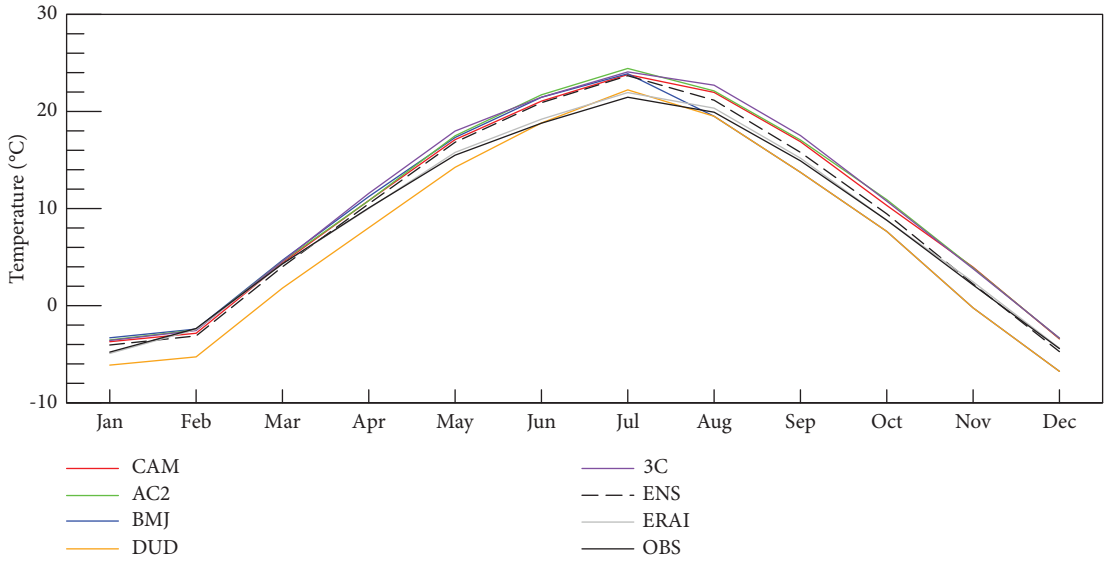

Figure 3: Annual cycle of monthly 2 m temperature: observations (black), ERA-Interim data (gray), and WRF simulations (colors).

As illustrated in Figure 4, most WRF configurations produce a warm bias, particularly during May–September, which can reach over 2°C. The only exception is EXP_DUD, which estimates clearly lower 2 m temperature than all other experiments. This might be attributed to that the Dudhia scheme is a very simple parameterization compared to other options for shortwave radiation scheme [44, 45]. The approach considered in this scheme is simpler than in other parameterizations because the radiative transfer equation as well as the spectral integration are not solved explicitly [46]. It corresponds well to the observation in summer while underestimates for other period along the year. The annual cycle is reproduced similarly by ERA-Interim and WRF.

3.1.3. Percentile Plot of Daily 2 m Temperature. All daily values are considered to calculate ten percentiles (1^{st}, 5^{th}, 10^{th}, 25^{th}, 50^{th}, 75^{th}, 90^{th}, 95^{th}, 99^{th}, and 99.9^{th}) for 2 m temperature. As shown in Figure 5, minor differences are observed among the explored configurations. The spread of WRF-simulated 2 m temperature with different physical options is generally less than 5°C.

In comparison with ERA-Interim, 2 m temperature within the range of 25%–75% is improved for most WRF simulations except EXP_DUD. Nevertheless, the extreme low and extreme high temperature are not improved or even worse for all WRF simulations. ERA-Interim seems to well describe the percentiles in the high temperature range (75^{th}, 90^{th}, 95^{th}, 99^{th}, and 99.9^{th}), while WRF simulates tend to produce a warmer extreme in summer. Both ERA-Interim and WRF underestimate the percentiles in low temperature range (1^{st}, 5^{th}, and 10^{th}), and cold bias in winter is larger in WRF simulations than ERA-Interim.

3.1.4. Time Series of Daily 2 m Temperature. To demonstrate skill in the simulation of temporal variability, area-averaged time series of daily average 2 m temperature over the Loess Plateau are presented as colored lines in Figure 6. The time series show that WRF is skillful at capturing the variability of the observed 2 m temperature. Nevertheless, biases can be identified, especially in summer and winter. In general, almost all the five configurations lead to warm bias during the period from Julian day 160–260. Significant negative bias can be identified for EXP_DUD, especially in winter period (Julian day 15–80 and 310–365).

3.2. Precipitation

3.2.1. Geographical Distribution of Precipitation Bias. Figures 2 and 7 provide an overview on the spatial distribution of the observed mean seasonal value and biases of ERA-Interim and WRF experiments for area-averaged

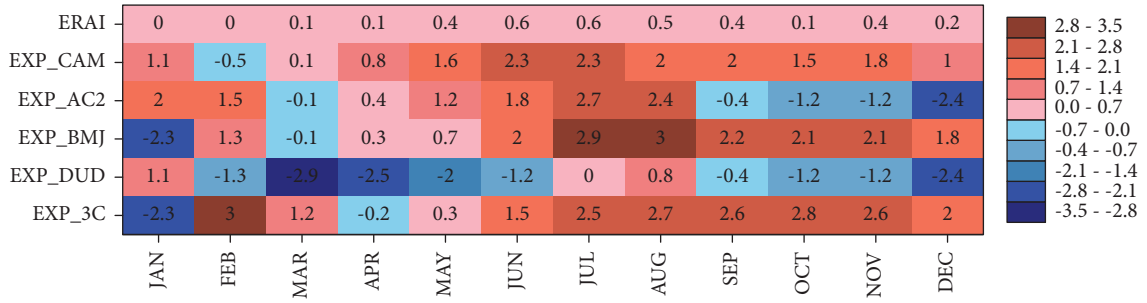

Figure 4: Monthly mean 2 m temperature bias of ERA-Interim and WRF simulations compared with CMFD-gridded observation. The unit is ˚C.

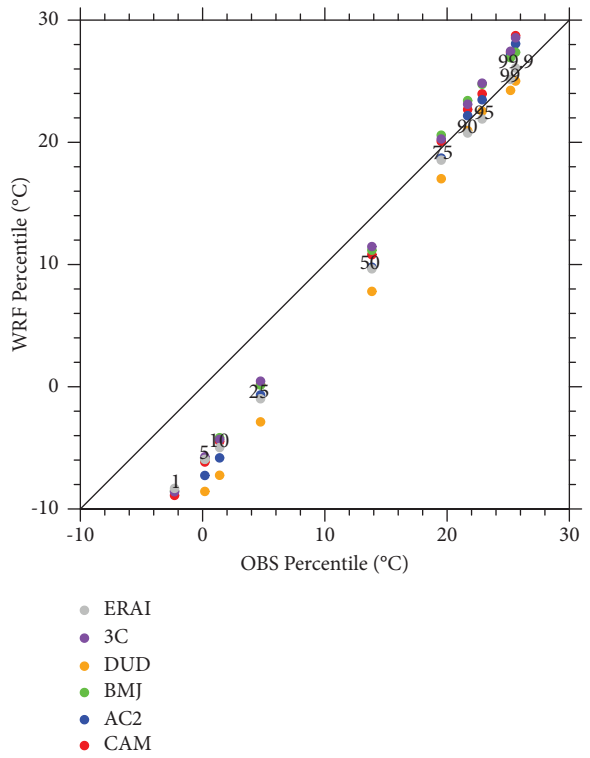

Figure 5: Daily 2 m temperature percentiles simulated by various WRF configurations and ERA-Interim vs. observational percentiles. Black line indicates a similar probability density function between models (WRF/ERA-Interim) and observations (CMFD).

precipitation. Observed precipitation shows clear seasonal difference, with highest amount in JJA and lowest in DJF. The precipitation gradient decreasing from southeast to northwest can be discerned from CMFD observation, particularly in JJA, SON, and MAM. The high rainfall center, located along the southern border, is prominent in these three seasons. Both ERA-Interim and WRF simulations generally reproduce the spatial variability precipitation for each season. Nevertheless, ERA-Interim generally presents dry bias over most parts of the plateau in MAM, JJA, and SON, while WRF simulations produce wet or dry bias depending on the season and location. In JJA, the WRF simulations present similar bias patterns (large wet bias) over SX province located in the eastern part of the plateau while different patterns in other parts of the plateau. For instance, EXP_DUD and EXP_AC2 similarly produce wet bias over almost the entire plateau (with the exception of the rainfall center area identified from the observation), with the extreme value over 3 mm/d. EXP_CAM, EXP_BMJ, and EXP_3C simulate dry bias over large area outside SX province (the eastern part). In DJF, MAM, and SON, the precipitation bias patterns by five WRF simulations are similar.

Similar to Table 3, the statistics of precipitation at seasonal scale for ERA-Interim reanalysis and each individual WRF experiments are summarized in Table 4. For WRF experiments, it can be identified that the correlation coefficients are much lower than that of 2 m temperature. They are among the range of 0.29–0.58, which are higher in MAM than other seasons. In SON, the correlations of WRF experiments are higher or equal than ERA-Interim while not in the case of DJF, MAM, and JJA. Unlike the dry bias of ERAI

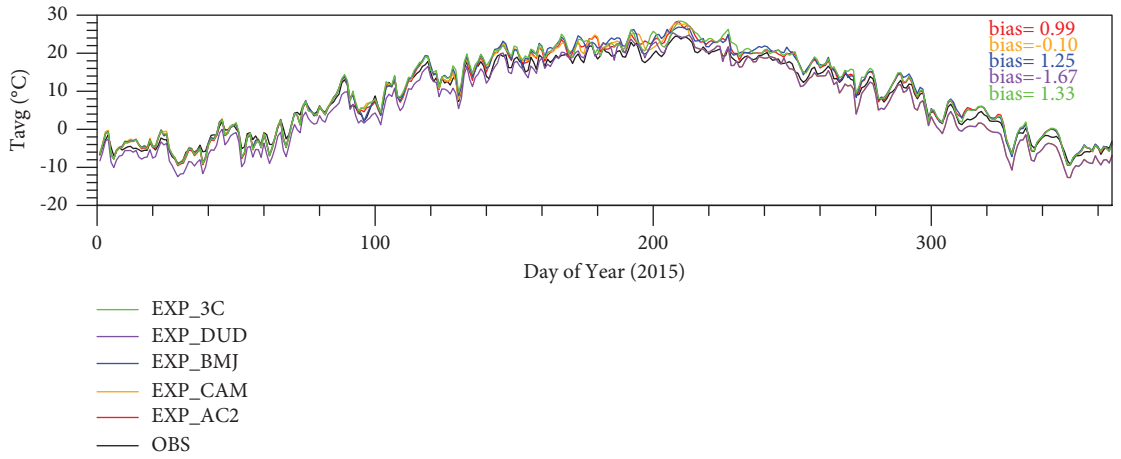

Figure 6: Area-averaged time series of daily average 2 m temperature from 1 January, 2015, to 31 December, 2015, over the Loess Plateau: observations (black) and WRF simulations (colors).

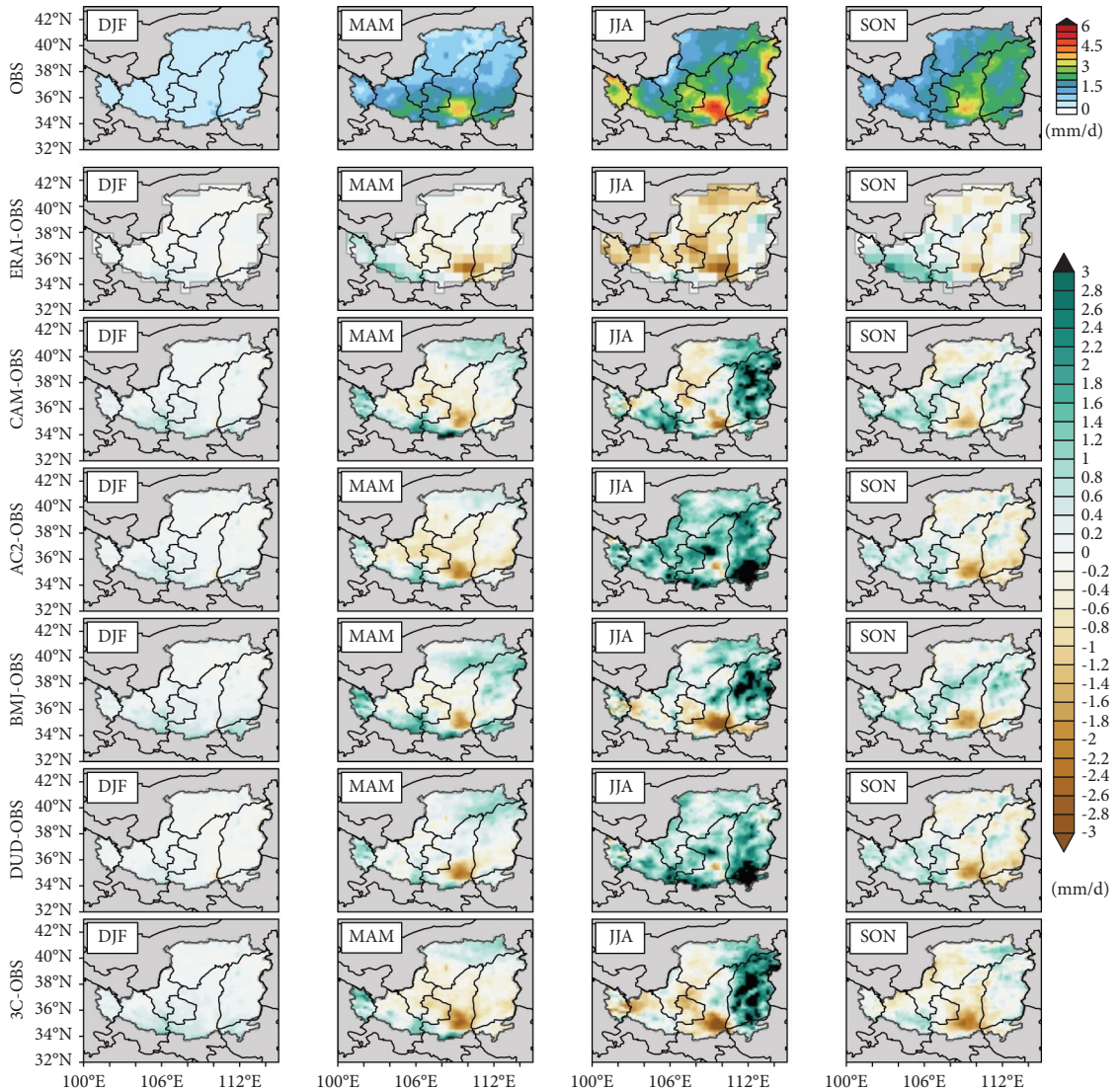

Figure 7: Seasonal mean observed precipitation and bias of ERA-Interim reanalysis and WRF simulations. The first row shows precipitation provided by the CMFD-gridded observation dataset as reference.

Table 4: Statistics of seasonal metrics for ERA-Interim reanalysis and WRF experiments in simulating daily precipitation.

	DJF			MAM			JJA			SON		
	BIAS	RMSE	CORR	BIAS	RMSE	CORR	BIAS	RMSE	CORR	BIAS	RMSE	CORR
ERA-Interim	0.01	0.02	0.40	−0.20	0.09	0.65	−0.79	0.16	0.67	−0.03	0.09	0.38
EXP_CAM	0.16	0.04	0.35	0.13	0.12	0.55	0.65	0.22	0.50	0.16	0.09	0.52
EXP_AC2	0.09	0.03	0.35	−0.19	0.10	0.62	1.42	0.28	0.57	−0.06	0.09	0.38
EXP_BMJ	0.16	0.04	0.37	0.34	0.12	0.57	0.48	0.22	0.29	0.21	0.10	0.47
EXP_DUD	0.04	0.02	0.33	0.16	0.09	0.58	1.11	0.24	0.60	−0.06	0.09	0.38
EXP_3C	0.19	0.04	0.41	−0.11	0.11	0.48	0.41	0.23	0.34	−0.16	0.09	0.48

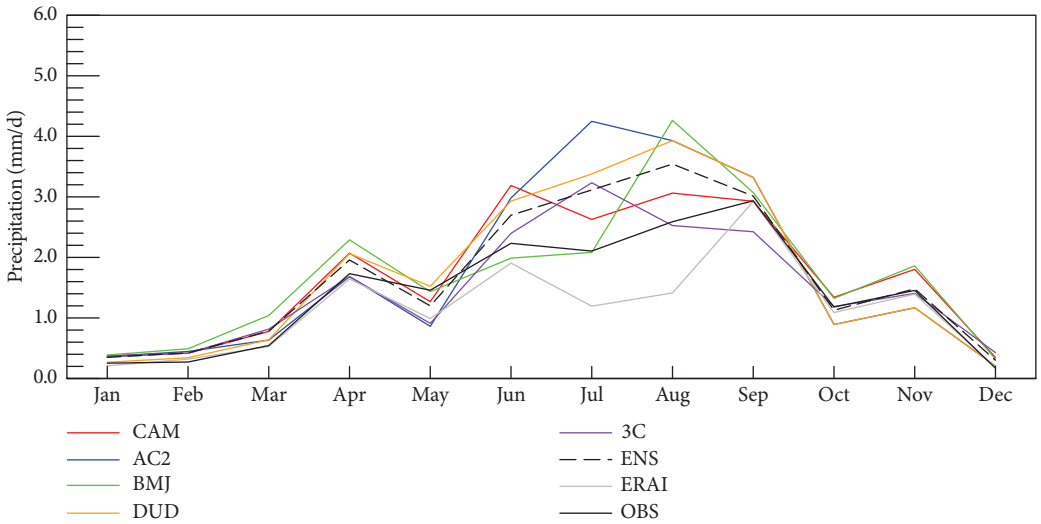

Figure 8: Annual cycle of monthly precipitation: observations (black), ERA-Interim data (gray), and WRF simulations (colors).

(−0.79 mm/d), wet biases dominate in summer (JJA) for all WRF experiments. EXP_AC2 holds the highest wet bias (1.42 mm/d), followed by EXP_DUD (1.11 mm/d).

3.2.2. Annual Cycle of Monthly Mean Precipitation. The annual cycles of WRF-simulated precipitation are presented in Figure 8, together with the observation and ERA-Interim data. In general, the seasonal pattern of rainfall rise is captured by the simulations, exhibiting high precipitation during summer and low during winter, with clear discrepancies in the rates. All the experiments capture the monthly variation during September–May with little intermodel variation.

As illustrated in Figure 9, EXP_BMJ holds the highest amount simulated, which clearly overestimates rainfall in this period. In summer, simulations varied, which broadly overestimate precipitation during JJA. EXP_AC2 and EXP_DUD simulate the highest precipitation amount in this period, prominently overestimate the amount. Interestingly, the fall from July to August is only captured by EXP_3C (Figure 8). Indeed, the modeling of precipitation is one of the main challenges in high-resolution regional models. Simulations of precipitation are less reliable compared with 2 m temperature. The WRF-simulated precipitation is generally higher than ERA-Interim, particularly in summer. It convinces the add value of dynamical downscaling.

3.2.3. Percentile Plot of Daily Precipitation. All daily values are taken into account to calculate eight percentiles (50^{th}, 60^{th}, 70^{th}, 75^{th}, 80^{th}, 90^{th}, 95^{th}, and 99^{th}) for precipitation. Figure 10 displays the percentiles for WRF, ERA-Interim, and observations. Estimations of precipitation show a clear underestimation for both WRF and ERA-Interim. The spread of WRF estimates in precipitation is larger for high percentile than low percentile, which indicates that the different choice of options is essentially important for extreme values.

In comparison with ERA-Interim, precipitation is improved for all combinations using WRF, which reduce the underestimation. The percentiles in the extreme high range are the greatest improved. This is in line with the description of the dynamical downscaling add-value, enhancement in characterizing extremes [1]. The best experiment in simulating precipitation within the range above 90^{th} is EXP_DUD and the best one among 70^{th} and 80^{th} is EXP_BMJ.

3.2.4. Taylor Diagram of Daily Precipitation. Statistical metrics for ERA-Interim and the five WRF experiments are computed for each season and displayed in Figure 11 as Taylor diagram in order to provide a synthetic summary how closely the WRF simulations match the observation. It indicates that simulated precipitation with a correlation

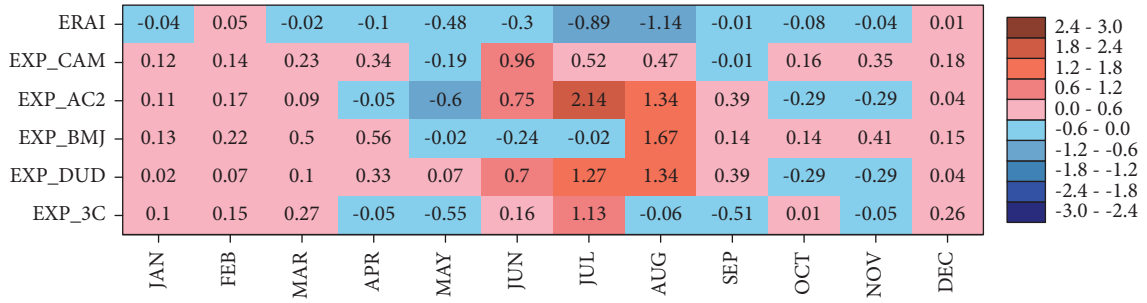

Figure 9: Monthly mean precipitation bias of ERA-Interim and WRF simulations compared with CMFD-gridded observation. The unit is mm/d.

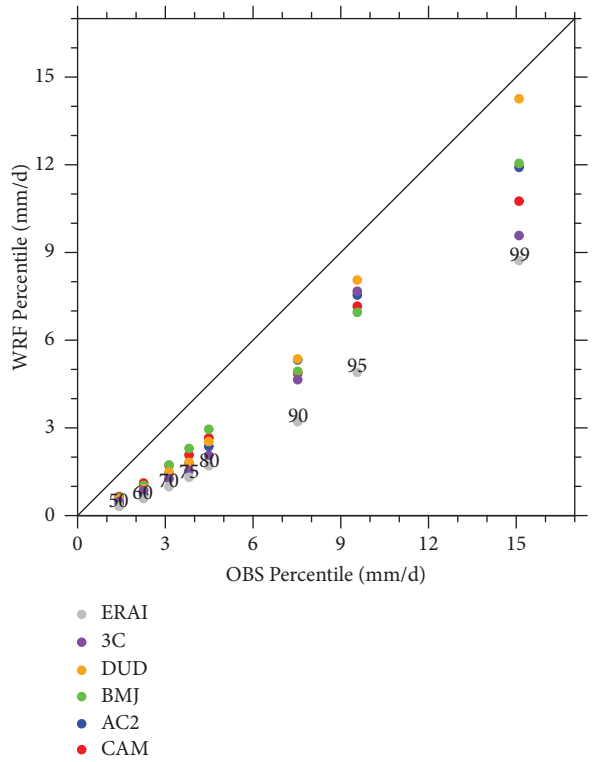

Figure 10: Daily precipitation percentiles simulated by various WRF configurations and ERA-Interim vs. observational percentiles. Black line indicates a similar probability density function between models (WRF/ERA-Interim) and observations (CMFD).

coefficient above 0.5 in MAM and SON and within the range between 0.3 and 0.5 in DJF and JJA. The correlations of WRF simulations are higher than ERA-Interim in JJA while comparable to ERA-Interim in other seasons. CRMSE is around 1.0 in MAM and SON, larger in JJA (2.0–4.0), and even greater in DJF (mostly above 4.0). It indicates that the variation is reasonably captured in MAM and SON while much higher in JJA and DJF, comparing with the observation. However, WRF simulations often generate higher CRMSE than ERA-Interim. It is difficult to identify the best physical combination since experiment performance varies among seasons. Generally, they cluster much more closely in MAM and SON while spread widely in DJF and JJA. EXP_DUD seems to be a fine choice when taking all three metrics into consideration for four seasons.

The relative low correlation coefficient indicates that satisfactory precipitation simulations over the Loess Plateau have remained a challenge. Precipitation is difficult to simulate due to complex physical processes and high spatial-temporal variability. Moreover, the topography effects in this hilly region also complex the simulation results.

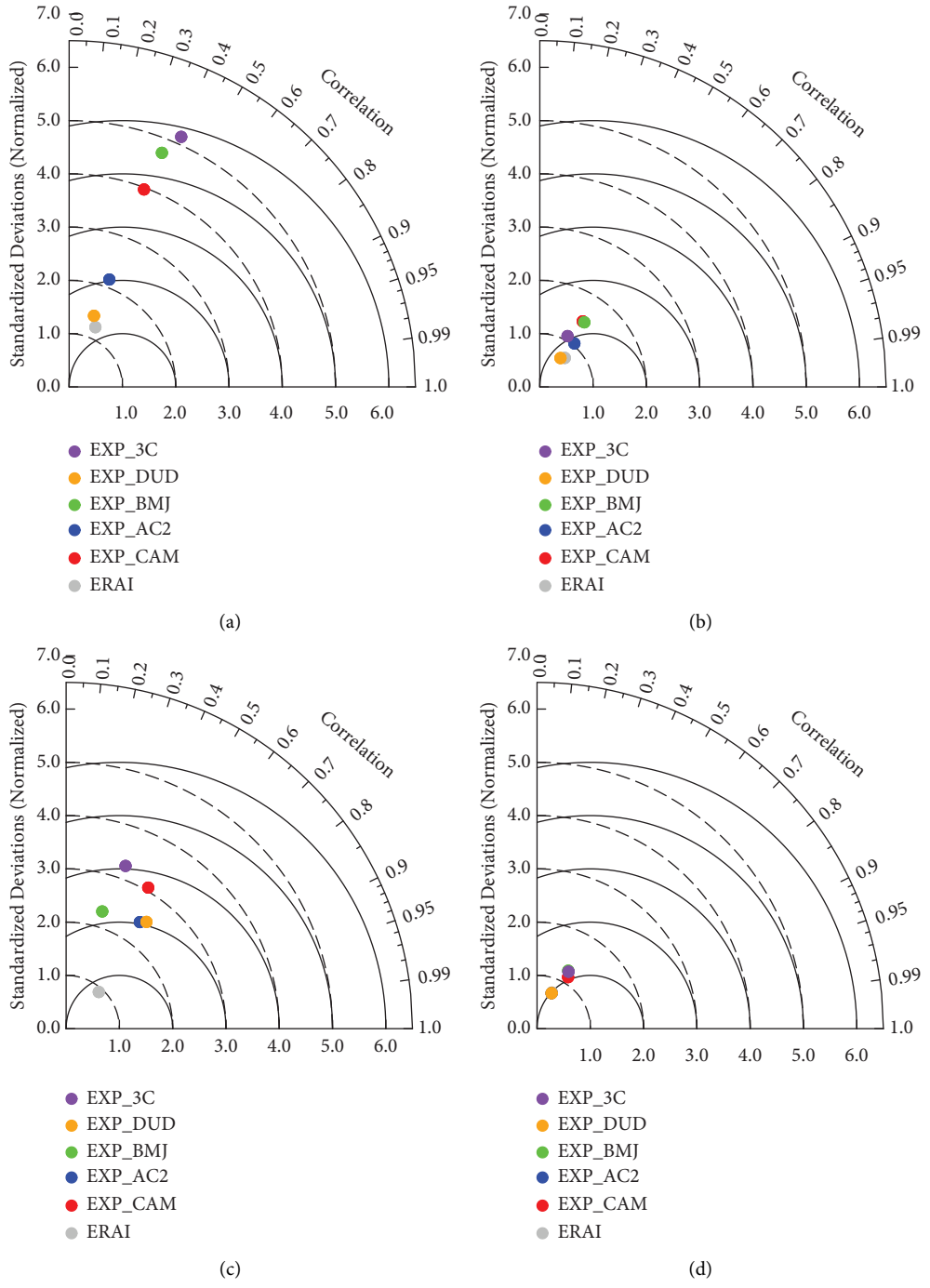

Figure 11: Taylor diagrams of area-averaged WRF simulation and ERA-Interim data with respect to observed precipitation in the year 2015 (full names of the individual experiment are given in Table 2) for (a) DJF (December–February), (b) MAM (March–May), (c) JJA (June–August), and (d) SON (September–November). Calculations are applied to present the temporal variability of daily precipitation. (Three statistics determine the relative places of the models: the Pearson's correlation coefficient (curved axes), the centered RMS error (gray contours), and the standard deviation (Oy-axis). The model fitting best with observations will lie the nearest to the Ox-axis.

4. Conclusion and Discussion

In this paper, regional climate simulations using WRF with different physical scheme options were carried out to produce one year long simulations over the Loess Plateau. The performances were evaluated against CMFD-gridded observational dataset, focusing on 2 m temperature and precipitation. The objective is to assess the general performance of the model and examine the sensitivity to different configurations. The results will provide useful information to select appropriate configuration over the Loess Plateau. The main conclusions are listed as follows:

(1) WRF simulations reproduce well the spatial variability of 2 m temperature for all seasons. Similar bias patterns can be identified for all experiments except EXP_DUD, which shows prominent cold bias over almost the entire plateau in DJF, MAM, and SON.

(2) WRF simulations reasonably capture the spatial variability of precipitation for all seasons, with large wet biases in summer. In JJA, the WRF simulations present similar bias patterns (large wet bias) over SX province located in the eastern part of the plateau while different patterns in other parts of the plateau.

(3) WRF simulations reproduce well observed monthly variation of 2 m temperature. However, most WRF configurations produce a warm bias, particularly during May–September, which can reach over 2°C. The only exception is EXP_DUD, which estimates clearly lower 2 m temperature than all other experiments.

(4) The seasonal pattern of rainfall rise is generally captured by the simulations, exhibiting high precipitation rate in summer and low value in winter. The WRF-simulated precipitation is generally higher than ERA-Interim, particularly in summer.

(5) At daily scale, minor differences are observed for 2 m temperature among the explored configurations. In comparison with ERA-Interim, 2 m temperature within the range of 25%–75% is improved for most combinations with the exception of EXP_DUD. Nevertheless, the extreme low and extreme high temperature are not improved or even worse for WRF simulations.

(6) As for daily precipitation, it is clearly underestimated for both WRF and ERA-Interim. In comparison with ERA-Interim, precipitation is improved for all combinations using WRF, which reduce the underestimation.

(7) Although it is difficult to choose one scheme as the best one for reproducing 2 m temperatures, the EXP-CAM simulation could be a good configuration, attending to the bias, although the rest of the experiments present similar results.

(8) As for precipitation, EXP_DUD seems to be a fine choice when taking all three metrics into consideration for four seasons.

A previous modeling study focuses on the Loess Plateau using RegCM [28] evaluated against CN05 dataset [47]. Their simulation tends to produce cold biases during winter and underestimate precipitation during summer. Our results are different with their conclusion, yet using different RCM model, configuration and gridded dataset compared. Some other studies have used WRF to simulate precipitation over China [29–31] or the Loess Plateau [32], and large wet biases are found over the plateau. Our simulation of dominant wet bias, particularly in summer, is broadly consistent with these results.

Numerous studies have been conducted worldwide with the WRF model to select the most appropriate configuration for regional climate simulations [37, 48–53]. From the common findings of these studies, it is evident that the WRF model is capable to represent regional climate although systematic biases can be identified in the simulations. Simulation performances have been found to be sensitive to physics parameterizations [11, 54–56] and land surface models [6, 57]. Optimal performance of WRF requires a computational expensive investigation over different combinations of parameterization schemes which vary from region to region.

It is important to point out several limitations in the present work. Due to limited computation resources, the period selected for simulation is only one year, which is not long enough to obtain climatic robust evidence. Interannual variation is not investigated since one year simulation outputs are analyzed. Our findings need to be further confirmed by future research with continuous simulation on a climatic (30 years) timescale.

Horizontal grid spacing is an issue which is worth to discuss. Numerous studies have addressed the numerical sensitivity to model grid spacing [58, 59]. Convection-permitting models (CPMs) are found to provide a better representation of convective processes on both climate and numerical weather prediction (NWP) timescales [60–71]. Although CPMs do not fully resolve convection, they can represent larger storms and mesoscale organization of convection explicitly on the model grid much better than the parameterizations of convection [72]. Future study will carry out simulations using CPMs at grid spacing less than ~5 km instead of 10 km, with computational cost taken into account.

In addition to physical configuration and grid spacing, the choice of domain location and geometry also impacts the model results [73–81]. Jones et al. [74] argued that the regional model domain should be larger than the region of interest to allow full development of small-scale features over the area of interest since a smaller domain size may suppress the development of key mesoscale features. In contrast to this, Bhaskaran et al. [75] showed that the regional model domain should not be so large that the simulation deviates significantly from the large-scale features of the driving model. The study by Seth and Giorgi [77] noticed in their study that the performance of a regional climate model is subjected to the careful selection of the domain for its specific application.

Another factor influencing the modeling results is model internal variability, which results from nonlinearities in the model physics and dynamics [82, 83]. It is defined as the difference between realization members where the only differences are the initial conditions. A multimember ensemble approach is commonly used by the regional climate modeling community to disentangle the reproducible and irreproducible components of climate variability [82, 84]. Some initial condition ensembles, commonly found in weather forecasting and climate modeling [85], have addressed internal variability within RCMs [82, 86–91].

Finally, due to limited computation resources, only five combinations of physical options were compared in the current study, generated by varying one option for each physical scheme from a reference configuration. To fully understand the impact of physical options, more combinations should be investigated.

Data Availability

The data that support the findings of this study are openly available. CMFD gridded dataset is accessible at https://data.tpdc.ac.cn. ERA-Interim surface air temperature and precipitation can be downloaded from https://cds.climate.copernicus.eu/.

Conflicts of Interest

The authors declare that they have no conflicts of interest.

Acknowledgments

The author would like to thank Dr. Werner at NCAR for her helpful advice on various technical issues relative to WRF simulation. All the model runs described in this study were carried out with the facilities of the Center for High Performance Computing at Wuhan University. This research was funded by the National Natural Science Foundation of China, grant number 42001359.

References

[1] F. Giorgi, "Regional climate modeling: status and perspectives," *Journal de Physique IV*.

[2] F. Giorgi, C. Jones, and G. Asrar, "Addressing climate information needs at the regional level: the CORDEX framework," *WMO Bull*, vol. 53, 2008.

[3] M. Rummukainen, "State-of-the-art with regional climate models," *WIREs Climate Change*, vol. 1, pp. 82–96, 2010.

[4] X. Z. Liang, H. I. Choi, K. E. Kunkel et al., "Surface boundary conditions for mesoscale regional climate models," *Earth Interactions*, vol. 9, no. 18, pp. 1–28, 2005.

[5] Y. Qian, S. J. Ghan, and L. R. Leung, "Downscaling hydroclimatic changes over the Western US based on CAM subgrid scheme and WRF regional climate simulations," *International Journal of Climatology*, vol. 30, no. 5, pp. 675–693, 2010.

[6] M. S. Bukovsky and D. J. Karoly, "Precipitation simulations using WRF as a nested regional climate model," *Journal of Applied Meteorology and Climatology*, vol. 48, no. 10, pp. 2152–2159, 2009.

[7] J. P. Evans and M. F. McCabe, "Regional climate simulation over Australia's Murray-Darling basin: a multitemporal assessment," *Journal of Geophysical Research: Atmospheres*, vol. 115, no. D14, 2010.

[8] E. J. Kim and S. Y. Hong, "Impact of air-sea interaction on East Asian summer monsoon climate in WRF," *Journal of Geophysical Research: Atmospheres*, vol. 115, no. D19, 2010.

[9] D. Argueso, J. M. Hidalgo-Munoz, S. R. Gamiz-Fortis, M. J. Esteban-Parra, J. Dudhia, and Y. Castro-Diez, "Evaluation of WRF parameterizations for climate studies over southern Spain using a multistep regionalization," *Journal of Climate*, vol. 24, no. 21, pp. 5633–5651, 2011.

[10] E. Flaounas, S. Bastin, and S. Janicot, "Regional climate modelling of the 2006 West African monsoon: sensitivity to convection and planetary boundary layer parameterisation using WRF," *Climate Dynamics*, vol. 36, no. 5-6, pp. 1083–1105, 2011.

[11] B. Pohl, J. Crétat, and P. Camberlin, "Testing WRF capability in simulating the atmospheric water cycle over Equatorial East Africa," *Climate Dynamics*, vol. 37, no. 7-8, pp. 1357–1379, 2011.

[12] J. Crétat, B. Pohl, Y. Richard, and P. Drobinski, "Uncertainties in simulating regional climate of Southern Africa: sensitivity to physical parameterizations using WRF," *Climate Dynamics*, vol. 38, no. 3-4, pp. 613–634, 2012.

[13] Á.J. Varga and H. Breuer, "Sensitivity of simulated temperature, precipitation, and global radiation to different WRF configurations over the Carpathian Basin for regional climate applications," *Climate Dynamics*, vol. 55, no. 9-10, pp. 2849–2866, 2020.

[14] J. P. Evans, M. Ekstrom, and F. Ji, "Evaluating the performance of a WRF physics ensemble over South-East Australia," *Climate Dynamics*, vol. 39, no. 6, pp. 1241–1258, 2012.

[15] Z. Li, F.-L. Zheng, W.-Z. Liu, and D. C. Flanagan, "Spatial distribution and temporal trends of extreme temperature and precipitation events on the Loess Plateau of China during 1961–2007," *Quaternary International*, vol. 226, no. 1-2, pp. 92–100, 2010.

[16] Q. Sun, C. Miao, Q. Duan, and Y. Wang, "Temperature and precipitation changes over the Loess Plateau between 1961 and 2011, based on high-density gauge observations," *Global and Planetary Change*, vol. 132, pp. 1–10, 2015.

[17] N. Herold, M. Ekström, J. Kala, J. Goldie, and J. P. Evans, "Australian climate extremes in the 21st century according to a regional climate model ensemble: implications for health and agriculture," *Weather and Climate Extremes*, vol. 20, pp. 54–68, 2018.

[18] J. Eitzinger, M. Trnka, D. SemerÁdovÁ et al., "Regional climate change impacts on agricultural crop production in Central and Eastern Europe – hotspots, regional differences and common trends," *The Journal of Agricultural Science*, vol. 151, no. 6, pp. 787–812, 2013.

[19] J. E. Olesen, T. R. Carter, C. H. Díaz-Ambrona et al., "Uncertainties in projected impacts of climate change on European agriculture and terrestrial ecosystems based on scenarios from regional climate models," *Climatic Change*, vol. 81, no. S1, pp. 123–143, 2007.

[20] S. Asseng, I. Foster, and N. C. Turner, "The impact of temperature variability on wheat yields," *Global Change Biology*, vol. 17, no. 2, pp. 997–1012, 2011.

[21] M. García-Valdecasas Ojeda, S. R. Gámiz-Fortis, Y. Castro-Díez, and M. J. Esteban-Parra, "Evaluation of WRF capability to detect dry and wet periods in Spain using drought indices,"

Journal of Geophysical Research: Atmospheres, vol. 122, no. 3, pp. 1569–1594, 2017.

[22] A. Halmstad, M. R. Najafi, and H. Moradkhani, "Analysis of precipitation extremes with the assessment of regional climate models over the Willamette River Basin, USA," *Hydrological Processes*, vol. 27, no. 18, pp. 2579–2590, 2013.

[23] W. Liu and T. Sang, "Potential productivity of the Miscanthus energy crop in the Loess Plateau of China under climate change," *Environmental Research Letters*, vol. 8, 2013.

[24] H. Zheng, C. Miao, D. Kong, J. Wu, and R. Zhou, "Changes in maximum daily runoff depth and suspended sediment yield on the Loess Plateau, China," *Journal of Hydrology*, vol. 583, 2020.

[25] Y. Deng, X. Wang, K. Wang et al., "Responses of vegetation greenness and carbon cycle to extreme droughts in China," *Agricultural and Forest Meteorology*, vol. 298-299, 2021.

[26] Y. F. Liu, Y. Liu, Z. H. Shi, M. López-Vicente, and G. L. Wu, "Effectiveness of re-vegetated forest and grassland on soil erosion control in the semi-arid Loess Plateau," *Catena*, vol. 195, 2020.

[27] J. Zhang, G. Gao, B. Fu et al., "A universal multifractal approach to assessment of spatiotemporal extreme precipitation over the Loess Plateau of China," *Hydrology and Earth System Sciences*, vol. 24, no. 2, pp. 809–826, 2020.

[28] L. Wang, K. K. W. Cheung, C. Y. Tam, A. P. K. Tai, and Y. B. Li, "Evaluation of the regional climate model over the Loess Plateau of China," *International Journal of Climatology*, vol. 38, no. 1, pp. 35–54, 2018.

[29] J. Bao, J. Feng, and Y. Wang, "Dynamical downscaling simulation and future projection of precipitation over China," *Journal of Geophysical Research: Atmospheres*, vol. 120, no. 16, pp. 8227–8243, 2015.

[30] S. Wang and E. Yu, "Simulation and projection of changes in rainy season precipitation over China using the WRF model," *Acta Meteorologica Sinica*, vol. 27, no. 4, pp. 577–584, 2013.

[31] E. Yu, H. Wang, Y. Gao, and J. Sun, "Impacts of cumulus convective parameterization schemes on summer monsoon precipitation simulation over China," *Acta Meteorologica Sinica*, vol. 25, no. 5, pp. 581–592, 2011.

[32] L. Tian, J. Jin, P. Wu, G.-Y. Niu, and C. Zhao, "High-resolution simulations of mean and extreme precipitation with WRF for the soil-erosive Loess Plateau," *Climate Dynamics*, vol. 54, no. 7-8, pp. 3489–3506, 2020.

[33] D. Wang, C. Menz, T. Simon, C. Simmer, and C. Ohlwein, "Regional dynamical downscaling with CCLM over East asia," *Meteorology and Atmospheric Physics*, vol. 121, no. 1-2, pp. 39–53, 2013.

[34] Y. En-Tao, W. Hui-Jun, and S. Jian-Qi, "A quick report on a dynamical downscaling simulation over China using the nested model," *Atmospheric and Oceanic Science Letters*, vol. 3, no. 6, pp. 325–329, 2010.

[35] C. Klein, D. Heinzeller, J. Bliefernicht, and H. Kunstmann, "Variability of West African monsoon patterns generated by a WRF multi-physics ensemble," *Climate Dynamics*, vol. 45, no. 9-10, pp. 2733–2755, 2015.

[36] Q. Yang, Z. Yu, J. Wei et al., "Performance of the WRF model in simulating intense precipitation events over the Hanjiang River Basin, China – a multi-physics ensemble approach," *Atmospheric Research*, vol. 248, 2021.

[37] D. Dai, L. Chen, Z. Ma, and Z. Xu, "Evaluation of the WRF physics ensemble using a multivariable integrated evaluation approach over the Haihe river basin in northern China," *Climate Dynamics*, vol. 57, no. 1-2, pp. 557–575, 2021.

[38] E. Katragkou, M. García-Díez, R. Vautard et al., "Regional climate hindcast simulations within EURO-CORDEX: evaluation of a WRF multi-physics ensemble," *Geoscientific Model Development*, vol. 8, no. 3, pp. 603–618, 2015.

[39] D. P. Dee, S. M. Uppala, A. J. Simmons et al., "The ERA-Interim reanalysis: configuration and performance of the data assimilation system," *Quarterly Journal of the Royal Meteorological Society*, vol. 137, no. 656, pp. 553–597, 2011.

[40] Q. Cao, J. Wu, D. Yu, and W. Wang, "The biophysical effects of the vegetation restoration program on regional climate metrics in the Loess Plateau, China," *Agricultural and Forest Meteorology*, vol. 268, pp. 169–180, 2019.

[41] J. He, K. Yang, W. Tang et al., "The first high-resolution meteorological forcing dataset for land process studies over China," *Scientific Data*, vol. 7, no. 1, p. 25, 2020.

[42] H. Gu and X. Wang, "Performance of the RegCM4.6 for high-resolution climate and extreme simulations over Tibetan plateau," *Atmosphere*, vol. 11, no. 10, p. 1104, 2020.

[43] K. E. Taylor, "Summarizing multiple aspects of model performance in a single diagram," *Journal of Geophysical Research: Atmospheres*, vol. 106, no. D7, pp. 7183–7192, 2001.

[44] J. Dudhia, "Numerical study of convection observed during the winter monsoon experiment using a mesoscale two-dimensional model," *Journal of the Atmospheric Sciences*, vol. 46, no. 20, pp. 3077–3107, 1989.

[45] J. Dudhia, "A history of mesoscale model development," *Asia-Pacific Journal of Atmospheric Sciences*, vol. 50, no. 1, pp. 121–131, 2014.

[46] A. M. Torrecillas, *A Study of the Shortwave Schemes in the Weather Research and Forecasting Model*, Doctoral dissertation, University of Barcelona, Barcelona, Spain, 2017.

[47] Y. Xu, X. Gao, Y. Shen, C. Xu, Y. Shi, and F. Giorgi, "A daily temperature dataset over China and its application in validating a RCM simulation," *Advances in Atmospheric Sciences*, vol. 26, no. 4, pp. 763–772, 2009.

[48] F. Ji, J. P. Evans, J. Teng, Y. Scorgie, D. Argüeso, and A. Di Luca, "Evaluation of long-term precipitation and temperature Weather Research and Forecasting simulations for southeast Australia," *Climate Research*, vol. 67, no. 2, pp. 99–115, 2016.

[49] T. B. Tariku and T. Y. Gan, "Sensitivity of the weather research and forecasting model to parameterization schemes for regional climate of Nile River Basin," *Climate Dynamics*, vol. 50, no. 11-12, pp. 4231–4247, 2018.

[50] X.-M. Hu, M. Xue, R. A. McPherson, E. Martin, D. H. Rosendahl, and L. Qiao, "Precipitation dynamical downscaling over the great plains," *Journal of Advances in Modeling Earth Systems*, vol. 10, no. 2, pp. 421–447, 2018.

[51] C.-C. Kuo and T. Y. Gan, "Estimation of precipitation and air temperature over western Canada using a regional climate model," *International Journal of Climatology*, vol. 38, no. 14, pp. 5125–5135, 2018.

[52] A. L. Hirsch, J. Kala, C. C. Carouge et al., "Evaluation of the CABLEv2.3.4 land surface model coupled to NU-WRFv3.9.1.1 in simulating temperature and precipitation means and extremes over CORDEX AustralAsia within a WRF physics ensemble," *Journal ofAdvances in Modeling Earth Systems*, vol. 11, no. 12, pp. 4466–4488, 2019.

[53] J. Kala, J. Andrys, T. J. Lyons, I. J. Foster, and B. J. Evans, "Sensitivity of WRF to driving data and physics options on a seasonal time-scale for the southwest of Western Australia," *Climate Dynamics*, vol. 44, no. 3-4, pp. 633–659, 2015.

[54] I.-J. Choi, E. K. Jin, J.-Y. Han, S.-Y. Kim, and Y. Kwon, "Sensitivity of diurnal variation in simulated precipitation during East Asian summer monsoon to cumulus

parameterization schemes," *Journal of Geophysical Research: Atmospheres*, vol. 120, no. 23, pp. 971–911, 2015.

[55] D. J. Gochis, W. J. Shuttleworth, and Z.-L. Yang, "Sensitivity of the modeled north American monsoon regional climate to convective parameterization," *Monthly Weather Review*, vol. 130, no. 5, pp. 1282–1298, 2002.

[56] B. Pohl, M. Rouault, and S. S. Roy, "Simulation of the annual and diurnal cycles of rainfall over South Africa by a regional climate model," *Climate Dynamics*, vol. 43, no. 7-8, pp. 2207–2226, 2014.

[57] F. Chen, C. Liu, J. Dudhia, and M. Chen, "A sensitivity study of high-resolution regional climate simulations to three land surface models over the western United States," *Journal of Geophysical Research: Atmospheres*, vol. 119, no. 12, pp. 7271–7291, 2014.

[58] B. Stevens, C. H. Moeng, A. S. Ackerman et al., "Evaluation of large-eddy simulations via observations of nocturnal marine stratocumulus," *Monthly Weather Review*, vol. 133, no. 6, pp. 1443–1462, 2005.

[59] S.-H. Jung, E.-S. Im, and S.-O. Han, "The effect of topography and sea surface temperature on heavy snowfall in the Yeongdong region: a case study with high resolution WRF simulation," *Asia-Pacific Journal of Atmospheric Sciences*, vol. 48, no. 3, pp. 259–273, 2012.

[60] J. Done, C. A. Davis, and M. Weisman, "The next generation of NWP: explicit forecasts of convection using the weather research and forecasting (WRF) model," *Atmospheric Science Letters*, vol. 5, no. 6, pp. 110–117, 2004.

[61] E. Richard, A. Buzzi, and G. Zängl, "Quantitative precipitation forecasting in the alps: the advances achieved by the mesoscale alpine programme," *Quarterly Journal of the Royal Meteorological Society*, vol. 133, no. 625, pp. 831–846, 2007.

[62] H. W. Lean, P. A. Clark, M. Dixon et al., "Characteristics of high-resolution versions of the met office unified model for forecasting convection over the United Kingdom," *Monthly Weather Review*, vol. 136, no. 9, pp. 3408–3424, 2008.

[63] M. L. Weisman, C. Davis, W. Wang, K. W. Manning, and J. B. Klemp, "Experiences with 0–36-h explicit convective forecasts with the WRF-ARW model," *Weather and Forecasting*, vol. 23, no. 3, pp. 407–437, 2008.

[64] T. Weusthoff, F. Ament, M. Arpagaus, and M. W. Rotach, "Assessing the benefits of convection-permitting models by neighborhood verification: examples from MAP D-PHASE," *Monthly Weather Review*, vol. 138, no. 9, pp. 3418–3433, 2010.

[65] E. J. Kendon, N. M. Roberts, C. A. Senior, and M. J. Roberts, "Realism of rainfall in a very high-resolution regional climate model," *Journal of Climate*, vol. 25, no. 17, pp. 5791–5806, 2012.

[66] A. F. Prein, A. Gobiet, M. Suklitsch et al., "Added value of convection permitting seasonal simulations," *Climate Dynamics*, vol. 41, no. 9-10, pp. 2655–2677, 2013.

[67] S. C. Chan, E. J. Kendon, H. J. Fowler, S. Blenkinsop, N. M. Roberts, and C. A. T. Ferro, "The value of high-resolution met office regional climate models in the simulation of multihourly precipitation extremes," *Journal of Climate*, vol. 27, no. 16, pp. 6155–6174, 2014.

[68] C. S. Schwartz, "Reproducing the september 2013 record-breaking rainfall over the Colorado front range with high-resolution WRF forecasts," *Weather and Forecasting*, vol. 29, no. 2, pp. 393–402, 2014.

[69] G. Fosser, S. Khodayar, and P. Berg, "Benefit of convection permitting climate model simulations in the representation of convective precipitation," *Climate Dynamics*, vol. 44, no. 1-2, pp. 45–60, 2015.

[70] P. Clark, N. Roberts, H. Lean, S. P. Ballard, and C. Charlton-Perez, "Convection-permitting models: a step-change in rainfall forecasting," *Meteorological Applications*, vol. 23, no. 2, pp. 165–181, 2016.

[71] C. Liu, K. Ikeda, R. Rasmussen et al., "Continental-scale convection-permitting modeling of the current and future climate of North America," *Climate Dynamics*, vol. 49, no. 1-2, pp. 71–95, 2017.

[72] G. Fosser, E. Kendon, S. Chan, A. Lock, N. Roberts, and M. Bush, "Optimal configuration and resolution for the first convection-permitting ensemble of climate projections over the United Kingdom," *International Journal of Climatology*, vol. 40, no. 7, pp. 3585–3606, 2020.

[73] R. A. Anthes, Y.-H. Kuo, E.-Y. Hsie, S. Low-Nam, and T. W. Bettge, "Estimation of skill and uncertainty in regional numerical models," *Quarterly Journal of the Royal Meteorological Society*, vol. 115, no. 488, pp. 763–806, 1989.

[74] R. G. Jones, J. M. Murphy, and M. Noguer, "Simulation of climate change over europe using a nested regional-climate model. I: assessment of control climate, including sensitivity to location of lateral boundaries," *Quarterly Journal of the Royal Meteorological Society*, vol. 121, no. 526, pp. 1413–1449, 1995.

[75] B. Bhaskaran, R. G. Jones, J. M. Murphy, and M. Noguer, "Simulations of the Indian summer monsoon using a nested regional climate model: domain size experiments," *Climate Dynamics*, vol. 12, no. 9, pp. 573–587, 1996.

[76] B. Bhaskaran, A. Ramachandran, R. Jones, and W. Moufouma-Okia, "Regional climate model applications on sub-regional scales over the Indian monsoon region: the role of domain size on downscaling uncertainty," *Journal of Geophysical Research: Atmospheres*, vol. 117, no. D10, 2012.

[77] A. Seth and F. Giorgi, "The effects of domain choice on summer precipitation simulation and sensitivity in a regional climate model," *Journal of Climate*, vol. 11, no. 10, pp. 2698–2712, 1998.

[78] B. Denis, R. Laprise, and D. Caya, "Sensitivity of a regional climate model to the resolution of the lateral boundary conditions," *Climate Dynamics*, vol. 20, no. 2, pp. 107–126, 2003.

[79] B. Denis, R. Laprise, D. Caya, and J. Côté, "Downscaling ability of one-way nested regional climate models: the Big-Brother Experiment," *Climate Dynamics*, vol. 18, no. 8, pp. 627–646, 2002.

[80] X. Gao, Y. Shi, D. Zhang et al., "Uncertainties in monsoon precipitation projections over China: results from two high-resolution RCM simulations," *Climate Research*, vol. 52, pp. 213–226, 2012.

[81] S. K. Dash, K. C. Pattnayak, S. K. Panda, D. Vaddi, and A. Mamgain, "Impact of domain size on the simulation of Indian summer monsoon in RegCM4 using mixed convection scheme and driven by HadGEM2," *Climate Dynamics*, vol. 44, no. 3-4, pp. 961–975, 2015.

[82] F. Giorgi and X. Bi, "A study of internal variability of a regional climate model," *Journal of Geophysical Research: Atmospheres*, vol. 105, no. D24, pp. 29503–29521, 2000.

[83] O. B. Christensen, M. A. Gaertner, J. A. Prego, and J. Polcher, "Internal variability of regional climate models," *Climate Dynamics*, vol. 17, no. 11, pp. 875–887, 2001.

[84] L. Separovic, R. de Elía, and R. Laprise, "Reproducible and irreproducible components in ensemble simulations with a regional climate model," *Monthly Weather Review*, vol. 136, no. 12, pp. 4942–4961, 2008.

[85] J. E. Kay, C. Deser, A. Phillips et al., "The community earth system model (cesm) large ensemble project: a community resource for studying climate change in the presence of internal climate variability," *Bulletin of the American Meteorological Society*, vol. 96, no. 8, pp. 1333–1349, 2015.

[86] P. N. J. Bonekamp, E. Collier, and W. W. Immerzeel, "The impact of spatial resolution, land use, and spinup time on resolving spatial precipitation patterns in the himalayas," *Journal of Hydrometeorology*, vol. 19, no. 10, pp. 1565–1581, 2018.

[87] J. Crétat, C. Macron, B. Pohl, and Y. Richard, "Quantifying internal variability in a regional climate model: a case study for Southern Africa," *Climate Dynamics*, vol. 37, no. 7-8, pp. 1335–1356, 2011.

[88] B. Fathalli, B. Pohl, T. Castel, and M. J. Safi, "Errors and uncertainties in regional climate simulations of rainfall variability over Tunisia: a multi-model and multi-member approach," *Climate Dynamics*, vol. 52, no. 1-2, pp. 335–361, 2019.

[89] R. Laprise, D. Kornic, M. Rapaić et al., "Considerations of domain size and large-scale driving for nested regional climate models: impact on internal variability and ability at developing small-scale details," in *Proceedings of Climate Change*, pp. 181–199, Springer, New York, NY, USA, 2012.

[90] P. Laux, P. N. B. Nguyen, J. Cullmann, T. P. Van, and H. Kunstmann, "How many RCM ensemble members provide confidence in the impact of land-use land cover change?" *International Journal of Climatology*, vol. 37, no. 4, pp. 2080–2100, 2017.

[91] P. Lucas-Picher, D. Caya, S. Biner, and R. Laprise, "Quantification of the lateral boundary forcing of a regional climate model using an aging tracer," *Monthly Weather Review*, vol. 136, no. 12, pp. 4980–4996, 2008.